The northern European shelf as increasing net sink for CO$_2$

Meike Becker[1,2], Are Olsen[1,2], Peter Landschützer[3], Abdirhaman Omar[4,2], Gregor Rehder[5], Christian Rödenbeck[6], and Ingunn Skjelvan[4,2]

[1]Geophysical Institute, University of Bergen, Bergen, Norway
[2]Bjerknes Center for Climate Research, Bergen, Norway
[3]Max Planck Institute for Meteorology, Hamburg, Germany
[4]NORCE Norwegian Research Centre AS, Bergen, Norway
[5]Leibniz Institute for Baltic Sea Reasearch, Warnemünde, Germany
[6]Max Planck Institute for Biogeochemistry, Jena, Germany

Correspondence: Meike Becker (meike.becker@uib.no)

Abstract. We developed a simple method to refine existing open ocean maps towards different coastal seas. Using a multi linear regression we produced monthly maps of surface ocean fCO$_2$ in the northern European coastal seas (North Sea, Baltic Sea, Norwegian Coast and in the Barents Sea) covering a time period from 1998 to 2016. A comparison with gridded SOCAT v5 data revealed standard deviations of the residuals $0\pm26\mu$atm in the North Sea, $0\pm16\mu$atm along the Norwegian Coast,

5     $0\pm19\mu$atm in the Barents Sea, and $2\pm42\mu$atm in the Baltic Sea. We used these maps as basis to investigate trends in fCO$_2$, pH and air-sea CO$_2$ flux. The surface ocean fCO$_2$ trends are smaller than the atmospheric trend in most of the studied region. Only the western part of the North Sea is showing an increase in fCO$_2$ close to 2 μatm yr^{-1}, which is similar to the atmospheric trend. The Baltic Sea does not show a significant trend. Here, the variability was much larger than possibly observable trends. Consistently, the pH trends were smaller than expected for an increase of fCO$_2$ in pace with the rise of atmospheric CO$_2$

10   levels. The calculated air-sea CO$_2$ fluxes revealed that most regions were net sinks for CO$_2$. Only the southern North Sea and the Baltic Sea emitted CO$_2$ to the atmosphere. Especially in the northern regions the sink strength increased during the studied period.

1   Introduction

15   For facing global challenges, such as predicting and tracking climate change, it is important to improve our understanding of the ocean carbon sink and its variability. Open oceans, especially those of the northern hemisphere, are relatively well understood and described in their large-scale variability (Gruber et al., 2019; Landschützer et al., 2018, 2019; Fay and McKinley, 2017). Reliable autonomous systems for measuring carbon dioxide partial pressure from commercial vessels were developed in the early 2000s (Pierrot et al., 2009) and have since been deployed on a large number of vessels (e.g. (Bakker et al., 2016). This has

20   resulted in sufficient data to develop methods to interpolate the data and to describe large scale air-sea CO$_2$ exchange and its

variability (Landschützer et al., 2014, 2013; Rödenbeck et al., 2013; Jones et al., 2015). These methods cover a wide variety of approaches, such as linear interpolations, machine learning, and model based estimates. By comparing the different results it is possible to achieve a good estimate of the uncertainty associated with the respective methods and to evaluate their performance relative to each other (Rödenbeck et al., 2015).

5   Despite coasts cover 7-10% of the world's oceans (Bourgeois et al., 2016), their contribution to the oceanic carbon sink is not yet fully constrained. Whether coastal oceans are a net sink or source for atmospheric CO_2 and how their role will change in a changing climate is still under debate (Bauer et al., 2013; Laruelle et al., 2010). Compared to the open ocean, longer time series and a higher spatial and temporal resolution of the observations are needed in order to capture all relevant coastal processes. Circulation patterns such as small currents caused by the topography, or tidal cycles result in a need for more complex maps

10   with a higher resolution (Bricheno et al., 2014; Lima and Wethey, 2012).These physical drivers are not the only reasons for coasts being more complicated to understand. Processes taking place in the sediments or respiration of sinking material do not directly affect the surface in the open ocean. In shallow coastal regions the water column can easily be mixed all the way to the bottom allowing for echange between the benthic and pelargic parts of the ecosystem (Griffiths et al., 2017).

       The different maps developed for describing the open ocean surface pCO_2 (CO_2 partial pressure) dynamics and air-sea CO_2

15   fluxes are not directly suitable for use in coastal regions. Many exclude data from coastal regions completely while all of them have a too coarse spatial resolution to properly resolve the coast with its small-scale variability (typically between 1 and 5 °). A few studies tried to describe coastal carbon dynamics but most of them had strong regional or temporal limitations. Table 1 shows an overview of studies with estimated pCO_2 trends over the northern European shelf while Table 2 presents available flux estimates. Laruelle et al. (2017) used a neural network approach to produce a global pCO_2 climatology of coastal oceans,

20   describing more distinct seasonal variability in the northern hemisphere than in the southern Pacific and Atlantic. Few studies attempted to constrain coastal air-sea fluxes before. Laruelle et al. (2018) published trend estimates in regions with a high data coverage based on winter data spanning up to 35 years finding the pCO_2 rise in coastal regions to lag behind the atmospheric rise in CO_2. For the Baltic Sea, Parard et al. (2016, 2017) used a neural network approach to produce surface ocean pCO_2 maps from 1998 to 2011 and estimated an air-sea flux of 1.2 mmol m^{-2} day^{-1}. Yasunaka et al. (2018) estimated a flux of

25   8 - 12 mmol m^{-2} day^{-1} in the Barents Sea and along the Norwegian coast using a self-organizing map technique. Most of the other available studies on the trends in coastal pCO_2 are based on data from either summer or winter. Estimates based on summer-only data typically show large interannual variations (Thomas et al., 2007; Salt et al., 2013), which led to the conclusion that here the interannual variability masks the actual long term trend. The approach to use winter-only data (Fröb et al., 2019; Omar et al., 2019), on the other hand, is based on the assumption that during this season the influence of biological

30   processes is negligible and therefore winter data can be used to establish a baseline trend. However, also using winter-only data has its drawbacks. In particular the choice of which months to include can cause biases and the optimal selection can differ from region to region .

       In this study we present a new approach to develop monthly fCO_2 (CO_2 fugacity) maps based on already existing open ocean pCO_2 maps, in four example regions: North Sea, Baltic Sea, Norwegian Coast and the Barents Sea, with the aim to determine

35   the air-sea CO_2 exchange in these regions and its decadal trends. A multi linear regression (MLR) was used, fitting driver data

Table 1. Overview of trends in surface ocean CO_2 reported in the literature.

	Reference	Time range	$dpCO_2/dt$ /μatm yr^{-1}
North Sea	Thomas et al. (2007)	2001-2005, summer data normalized to 16°	7.9
North Sea	Salt et al. (2013)	2001-2005, summer data, normalized to 16°	6.5
North Sea	Salt et al. (2013)	2005-2008, summer data, normalized to 16°	1.33
Faeroe Banks	Fröb et al. (2019)	2004-2017, winter data	2.25 ± 0.20
North Sea, west	Omar et al. (2019)	2004-2017, winter data	2.19 ± 0.55
North Sea, east	Omar et al. (2019)	2004-2017, winter data	not significant
North Sea	Laruelle et al. (2018)	1988-2015	almost no trend
English channel	Laruelle et al. (2018)	1988-2015	slightly smaller than atmosphere
Baltic Sea	Wesslander et al. (2010)	1994-2008	larger than atmosphere
Baltic Sea	Schneider and Müller (2018)	2008-2015	4.6 - 6.1
Baltic Sea, west	Laruelle et al. (2018)	1988-2015	much smaller than atmosphere, slightly negative
Barents Sea	Yasunaka et al. (2018)	1997-2013	not significant
Barents Sea	Laruelle et al. (2018)	1988-2015	about the same as atmosphere
Atmosphere	global average	1997-2016	2.02 ppm yr^{-1}

Table 2. Overview of air-sea CO_2 fluxes reported in the literature. Negative sign denotes flux from atmosphere to ocean.

	Reference	Time range	F / mmol m^{-2} day^{-1}
North Sea	Meyer et al. (2018)	2001/2002	-3.8
Baltic Sea	Parard et al. (2017)	1998-2011	1.2
Norwegian Coast	Yasunaka et al. (2018)	1997-2013	-4 - -8
Barents Sea	Yasunaka et al. (2018)	1997-2013	-8 - -12

against $f\mathrm{CO_2}$ observations. Based on the resulting $f\mathrm{CO_2}$ maps and a salinity-alkalinity correlation we also produced monthly maps of coastal pH. The performance of the produced maps was evaluated and the maps were then used to investigate trends in coastal $f\mathrm{CO_2}$ and pH in the entire region from 1998 to 2016. Finally, we calculated air-sea $\mathrm{CO_2}$ fluxes and show their temporal and spatial patterns.

2 Method

2.1 Study area

This work focuses on northern European coasts and marginal seas. As we want to show the performance of the MLR method we picked a number of regions with very different characteristics: the North Sea, the Baltic Sea, the Norwegian coast and the western Barents Sea. We decided on these regions specifically because (1) the data coverage in these regions is fairly high and (2) the authors have strong knowledge on the specific regions. This is important in order to properly evaluate the maps and to assess whether or not the output is realistic. The 4 regions were defined based on the COastal Segmentation and related CATchments (COSCAT) segmentation scheme (Laruelle et al., 2013). The threshold for defining a region as coastal was set to a depth limit of $500\,\mathrm{m}$ (Figure 1). By using this definition, we produce an overlap to the open ocean maps, allowing our maps to be merged with the open ocean maps.

2.2 Data handling

The $\mathrm{CO_2}$ data used in this study were extracted from SOCAT version 5 (Bakker et al., 2016). Their coverage is shown in Figure 2. An overview over the reanalysis products used as driver data is given in Table 3. We use as basic driver data sea surface temperature (SST), sea surface salinity (SSS), chlorophyll a concentration (Chl a), mixed layer depth (MLD), bathymetry (BAT), distance from shore (DIST), ice concentration (ICE), the change in ice concentration from month to month. Chl a values during the dark winter season were set to 0. In addition to the reanalysis data, $p\mathrm{CO_2}$ values from the closest coastal grid cell of the open ocean map was used as a driver in our MLR. We can neglect the difference between partial pressure and fugacity of $\mathrm{CO_2}$ (about 1 μatm) at this place as it is much smaller than the accuracy of the data extracted from SOCAT v5 (2 to 10 μatm) and the uncertainty associated to the open ocean maps. The open ocean $p\mathrm{CO_2}$ values were extracted from two different products (Rödenbeck et al. (2014) (version oc_v1.5) and Landschützer et al. (2017, 2016) (version 2016)). Rödenbeck et al. (2014) is based on a data-driven diagnostic model of ocean biogeochemistry fitted against surface $p\mathrm{CO_2}$ observations while Landschützer et al. (2016) is based on a two-step neural network (a feed-forward network coupled with self-organizing maps, FFN-SOM) trained with the $p\mathrm{CO_2}$ observations. Please note that the Rödenbeck open ocean map also contains data in coastal grid boxes, while the Landschützer open ocean map is restricted to the open ocean regions south of 80°N. The MLR models based on these two are called MLR 1 (based on the coastal $p\mathrm{CO_2}$ values from the Rödenbeck map) and MLR 2 (based on the the nearest open ocean $p\mathrm{CO_2}$ values of the Landschützer map), respectively. To determine the extent to which the regressions

Table 3. Products used as driver data in the MLR and the maps.

Product used	Resolution	Reference
Chl a for MLR	4km x 4km, 8 days	Global Ocean Chlorophyll (Copernicus-GlobColour)
		from Satellite Observations - Reprocessed
Chl a for maps	4km x 4km, monthly	Global Ocean Chlorophyll (Copernicus-GlobColour)
		from Satellite Observations - Reprocessed
MLD	12.5km x 12.5km, monthly	Arctic Ocean Physics Reanalysis
ICE	$0.25°x0.25°$, monthly	Cavalieri et al. (1996)
SST / SSS	$0.25°x0.25°$, weekly	Global Ocean Observation-based Products
		Global_Rep_Phy_001_021
BAT	2min x 2min	ETOPO2v2 Center (2006)
Rödenbeck pCO_2	$5° \times 4°$, monthly	Rödenbeck et al. (2014)
Landschützer pCO_2	$1° \times 1°$, monthly	Landschützer et al. (2017)

benefit from the information in the open ocean maps, a third MLR, MLR 3, was determined. This does not have any of the open ocean maps as driver, but instead uses the year as proxy for the annual rise in CO_2.

For producing the input data for the MLR, each SOCAT $f CO_2$ data point was assigned to the closest data point in space and time of each of the reanalysis data. This produces a matrix as long as the SOCAT $f CO_2$ observations for each driver data.

5 After this, the $f CO_2$ data as well as all driver data were binned on a monthly $0.125°x0.125°$ grid covering 1998 to 2016. This step ensures that the driver data have the same bias in space and time within each grid box as the $f CO_2$ data. If a grid box for example only contains observations from the first week of the month and the northwestern corner, we make sure, that also the gridded driver data only contains values from the first week and the northwestern corner of the grid box, and not an average over the entire month and grid box. This is mostly important for the chlorophyll driver data, which are available in a very high

10 resolution compared to the $f CO_2$ maps produced in this work. These driver data were used for the MLR.

For producing the final maps, a second set of the driver data was produced, in the following called field data. Here the driver data were directly regridded to a monthly $0.125°x0.125°$ grid, providing the full spatial and temporal coverage and a homogene average in each grid box. The field data were used to produce the $f CO_2$ maps based on the equation derived from the MLR.

2.3 Multi linear regression

15 The multi linear regression models were constructed by forward and backward stepwise regression using the driver data as predictor variables to model the $f CO_2$ observations. During a stepwise regression in each step, a variable is tested for being added or removed from the set of explanatory variables. This decision on whether to add or remove a term was based on the p-value of the F-statistic with or without the term in question. The entrance tolerance was set to 0.05 and the exit tolerance to
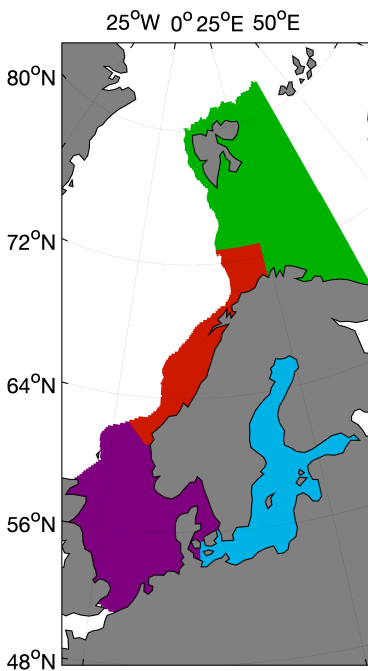
Figure 1. The study area and the location of the four different regions North Sea (purple), Norwegian Coast (red), Barents Sea (green) and Baltic Sea (blue).
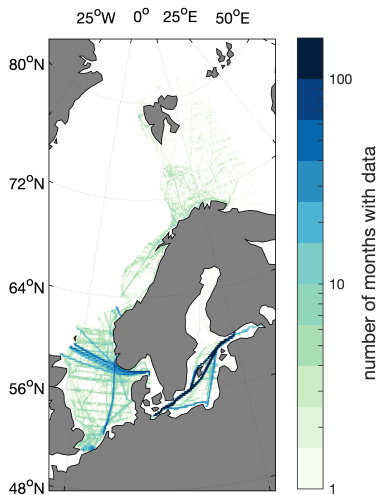
Figure 2. The number of months with $f\text{CO}_2$ data from SOCAT v5 in each grid box.

Table 4. Driver used in the different regressions.

	MLD	SST	SSS	CHL	ICE	ICE change	BAT	DIST	pCO$_2$	year
North Sea										
MLR 1	x	x	x	x	x		x		x	
MLR 2	x	x	x	x	x	x	x	x	x	
MLR 3	x	x	x	x	x	x	x	x		x
Norwegian Coast										
MLR 1	x	x	x	x	x		x		x	
MLR 2	x	x	x	x	x	x	x		x	
MLR 3	x	x	x	x	x	x	x			x
Barents Sea										
MLR 1	x	x	x	x	x	x	x		x	
MLR 2	x	x	x	x	x	x	x		x	
MLR 3	x	x	x	x	x	x	x			x
Baltic Sea										
MLR 1	x	x	x	x	x	x	x		x	
MLR 2	x	x	x	x	x	x	x		x	
MLR 3	x	x	x	x	x		x			x

0.1. The model includes constant, linear, and quadratic terms as well as products of linear terms. Equation 1 gives the basic equation, with $X_1...X_n$ being the driver data and $a_1...a_{nn}$ the regression coefficients.

$$y = a_0 + a_1 \cdot X_1 + ... + a_n \cdot X_n + a_{12} \cdot X_1 X_2 + ... + a_{mn} \cdot X_m X_n + a_{11} \cdot X_1^2 + ... + a_{nn} \cdot X_n^2 \qquad (1)$$

The pCO$_2$ value of the respective open ocean maps (MLR 1 and MLR 2), or the year were added (MLR 3). Inclusion of
5   stationary drivers (such as month, latitude and longitude) in the MLR increased the performance of MLR 2 and MLR 3. However, these were still not better than MLR 1 and we therefore decided to limit this analysis to dynamic parameters. Using dynamic drivers only assures a dynamic description of the conditions in the field, and gives us the possibility to reproduce changes caused by a regime shifts, for example the ongoing atlanticfication of the Barents Sea (Oziel et al., 2016; Lind et al., 2018).

10   **2.4 Validation**

The three linear fits were compared to each other by taking into account the R^2 and the root mean square error (RMSE) of the fit, and the Nash Sutcliffe method efficiency (ME) (Nondal et al., 2009). The method efficiency compares how well the

model output (E_n) fits the observations (I_n) for every data point n to how well a simple monthly average ($\overline{I}$) would fit the observations:

$$\mathrm{ME} = \frac{\sum_n \left(I_\mathrm{n} - E_\mathrm{n}\right)^2}{\sum_n \left(I_\mathrm{n} - \bar{\mathrm{I}}\right)^2} \tag{2}$$

A method efficiency >1 means that using just monthly averages of all data in the region would fit better to measured data
5 than the respective model, Generally, a method efficiency >0.8 is considered bad. Besides the statistics of the fit itself, the final maps were also compared to the gridded SOCAT v5 data, resulting in an average offset and standard deviation. In order to compare the maps against data that were not used to produce the maps, we predicted the $f\mathrm{CO}_2$ for the years 2017 and 2018 (ie, we applied the trained multi-linear model to driver data from 2017 and 2018) and compared these maps to $f\mathrm{CO}_2$ observations in SOCAT v2019, gridded on a monthly $0.125°\mathrm{x}0.125°$ grid. We also compare the map directly with observations at two time
10 series in the North Sea and the Baltic Sea.

2.5 Ocean acidification

For calculating ocean acidification, alkalinity (AT) was estimated in the North Sea, along the Norwegian Coast, and in the Barents Sea via a salinity-alkalinity correlation after Nondal et al. (2009). Alkalinity describes the capacity of the sea water to buffer changes in pH. As the concentration of most of the weak acids in seawater is strongly dependent on the salinity, alkalinity
15 can in many regions be estimated from salinity. However, in regions with a high amount of organic acids in seawater, for example in strong blooms or at river moths, deviations from the alkalinity-salinity relationship can be observed. The carbonate system was calculated using the CO2SYS program (van Heuven et al., 2009) with carbonic acid dissociation constants of Mehrbach et al. (1973) as refitted by Dickson and Millero (1987) and KSO_4^- dissociation constants after Dickson (1990). For the Baltic Sea, we did not calculate pH as the alkalinity-salinity relationship in this region is complex due to different AT-S
20 relations in different sub-regions of the Baltic Sea, and a non-negligible increase of AT over the last 25 years (Müller et al., 2016).

2.6 Calculation of trends

For calculating trends of $f\mathrm{CO}_2$ and ocean acidification, the data in every grid box were deseasonalised by subtracting the long-term averages of the respective months. Then a linear fit was applied to the deseasonalised time-series. For illustrating the
25 influence of interannual variability we calculated the trend for different time ranges. As a time range less than 10 years barely resulted in significant trends, we decided to limit the trend analysis to starting years from 1998 to 2006 and ending years from 2008 to 2016.

2.7 Flux calculation

The air-sea disequilibrium was calculated as the difference between our mapped $f\mathrm{CO}_2$ values and atmospheric $f\mathrm{CO}_2$ in each
30 grid cell and time step. The atmospheric $f\mathrm{CO}_2$ was determined by converting the $x\mathrm{CO}_2$ from the NOAA Marine Boundary

Layer Reference product from the NOAA GMD Carbon Cycle Group into $f\mathrm{CO}_2$ by using the monthly SST and SSS data (Table 3) and monthly air pressure data from the NCEP-DOE Reanalysis 2 (?). We calculated the air-sea CO_2 flux (F) according to Equation 3, such that negative fluxes are into the ocean. The gas transfer coefficient k was determined using the quadratic wind speed (u) dependency of Wanninkhof (2014) (Equation 4). The Schmidt number, Sc, was calculated according to Wanninkhof
5 (2014) and the solubility coefficient for CO_2, K_0, after Weiss (1974).

$$\mathrm{F} = k \cdot K_0 \cdot (f\mathrm{CO}_{2,\mathrm{sw}} - f\mathrm{CO}_{2,\mathrm{atm}}) \tag{3}$$

$$k = a_q \cdot \langle u^2 \rangle \cdot \left(\frac{Sc}{660} \right)^{-0.5} \tag{4}$$

In our calculations, we used 6-hourly winds of the NCEP-DOE Reanalysis 2 product. The coefficient a_q in Equation 4
10 is strongly dependent on the used wind product. We determined it to be $a_q = 0.16 \mathrm{cmh}^{-1}$ for the 6-hourly NCEP 2 product following the recommendations of Naegler (2009) and by using the World Ocean Atlas sea surface temperatures (Locarnini et al., 2018). The barrier effect of sea ice on the flux was taken into account by relating the flux to the degree of ice cover following of Loose et al. (2009). As the gas exchange in areas that are considered 100% ice covered from satellite images should not be completely neglected, we use a sea ice barrier effect for a 99% sea ice cover in all grid cells where the sea ice
15 coverage exceeded 99%.

3 Results

3.1 Maps of $f\mathrm{CO}_2$

The skill assessment metrics for MLR 1, MLR 2 and MLR 3 are presented in Table 5. It shows the the R^2 and RMSE of the fit, the ME, as well as the average offset and standard deviation to the gridded SOCAT data. The MLRs substantially improve the
20 predictions of the open ocean maps in all studied regions, showing a better average offset and standard deviation to SOCAT v5 and ME than the coarser-resolution open ocean maps (for example: Rödenbeck map: North Sea 0 ± 95 μatm, Norwegian Coast: 2 ± 17 μatm, Barents Sea: 22 ± 40 μatm, Baltic Sea: 4 ± 48 μatm; MLD1: North Sea: 0 ± 26 μatm, Norwegian Coast: 0 ± 16 μatm, Barents Sea: 0 ± 19 μatm,Baltic Sea: 2 ± 42 μatm). In all regions MLR 1 was performing best, showing also the best model efficiency, the highest R^2 and the smallest RMSE of the fit, while MLR 2 and MLR 3 showed a weaker performance.
25 This can be explained by the fact that the Rödenbeck map contains also information about the coasts and the Barents Sea, while for MLR 2 the closest open ocean grid cell of Landschützer et al. (2017) was used. MLR 3 showed the weakest performance, which shows the value of using information from the open ocean maps in the regression.

Figure 3 shows, from left to right, the spatial distribution of the average difference between the predicted $f\mathrm{CO}_2$ by MLR1 and the gridded SOCAT v5 data, the Rödenbeck map and the gridded SOCAT v5 data, the difference between MLR 1 and the
30 Rödenbeck map, and, for comparison, between MLR 3 and the SOCAT v5 data. In the North Sea, MLR 1 seems to slightly overestimate the $f\mathrm{CO}_2$ in the constantly mixed region at the entrance of the English channel and the area off the Danish North
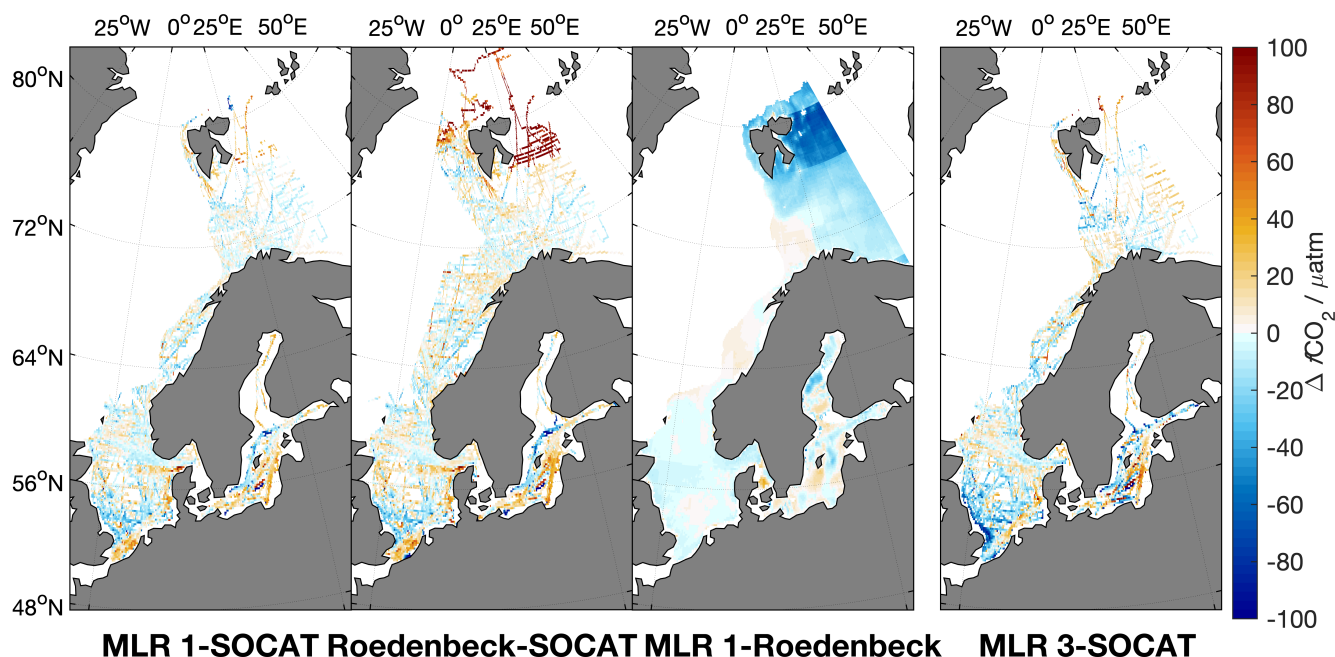
Figure 3. Average regional differences between MLR 1 and gridded SOCAT v5 data, the Rödenbeck map and gridded SOCAT v5 data, MLR 1 and the Rödenbeck map, and MLR 3 and the gridded SOCAT v5 data (from left to right).

Sea coast. In the Baltic, MLR 1 generally describes well the spatial variability in $f\mathrm{CO}_2$. In the Gulf of Finland it usually predicts too low $f\mathrm{CO}_2$ values during May/June while MLR 1 slightly underestimates events of very high $f\mathrm{CO}_2$ in December/January. However, it shows lower spatial biases than the original Rödenbeck map. MLD 2 and 3 are showing much larger differences from SOCAT v5 data, especially in the Baltic Sea and the southern North Sea. Therefore, we will use MLR 1 in the further

5 analysis. An extended validation of the MLR 1 maps can be found in the discussion section.

Figure 4 shows the monthly averages of $f\mathrm{CO}_2$ produced by MLR 1 for February, May, August and November. In all regions, the highest $f\mathrm{CO}_2$ values occur in the winter, while the lowest $f\mathrm{CO}_2$ occur in summer. The largest seasonal cycle could be observed in the Baltic Sea, where $f\mathrm{CO}_2$ reached well below 200 μatm in mid summer and over 500 μatm during the winter.

3.2 Maps of pH

10 The monthly average of pH calculated from MLR 1 $f\mathrm{CO}_2$ is ranging from about 8 during winter to 8.15 during summer in the North Sea and at the Norwegian coast (Figure 5). Towards the Barents Sea the pH maximum increases during summer to 8.2. The pH of 8.00 - 8.15 in regions with a large influence from the Atlantic, such as the northern North Sea and the Norwegian coast, is in good agreement with the range of pH determined for the open North Atlantic (Lauvset and Gruber, 2014; Lauvset

Table 5. Statistical evaluation of the MLR 1, MLR 2 and MLR 3 in comparison to the open ocean maps of Rödenbeck et al. (2015) and Landschützer et al. (2017) for each region. The data for the open ocean map of Landschützer et al. (2017) are in parentheses since this is based on an extrapolation of he closed open ocean grid cell towards the coast. The number of grid cells containing data is given behind the region abbreviations.

	R^2 adj	RMSE	ME median	difference to gridded SOCAT v5	
				mean	standard deviation
		/μatm		/μatm	/μatm
North Sea (36170)					
MLR 1	0.7271	25	0.3145	-0.15	26
MLR 2	0.5130	33	0.5789	-0.52	36
MLR 3	0.5331	33	0.4895	-2.4	32
Rödenbeck			0.3522	-0.28	95
(Landschützer)			0.5714	-4.7	103
Norwegian Coast (16014)					
MLR 1	0.7860	16	0.1742	0.46	16
MLR 2	0.5634	22	0.3597	-2.3	24
MLR 3	0.6074	20	0.2436	-0.08	21
Rödenbeck			0.2177	2.0	17
(Landschützer)			0.3294	7.0	23
Barents Sea (13925)					
MLR 1	0.8871	12	0.1069	0.32	19
MLR 2	0.8724	14	0.0986	1.3	68
MLR 3	0.8672	18	0.1082	1.3	24
Rödenbeck			0.2923	22	40
(Landschützer)			0.3364	15	44
Baltic Sea (46810)					
MLR 1	0.9076	39	0.0488	2.2	42
MLR 2	0.6733	66	0.3111	-1.0	68
MLR 3	0.6628	67	0.3027	0.24	69
Rödenbeck			0.1326	4.2	48
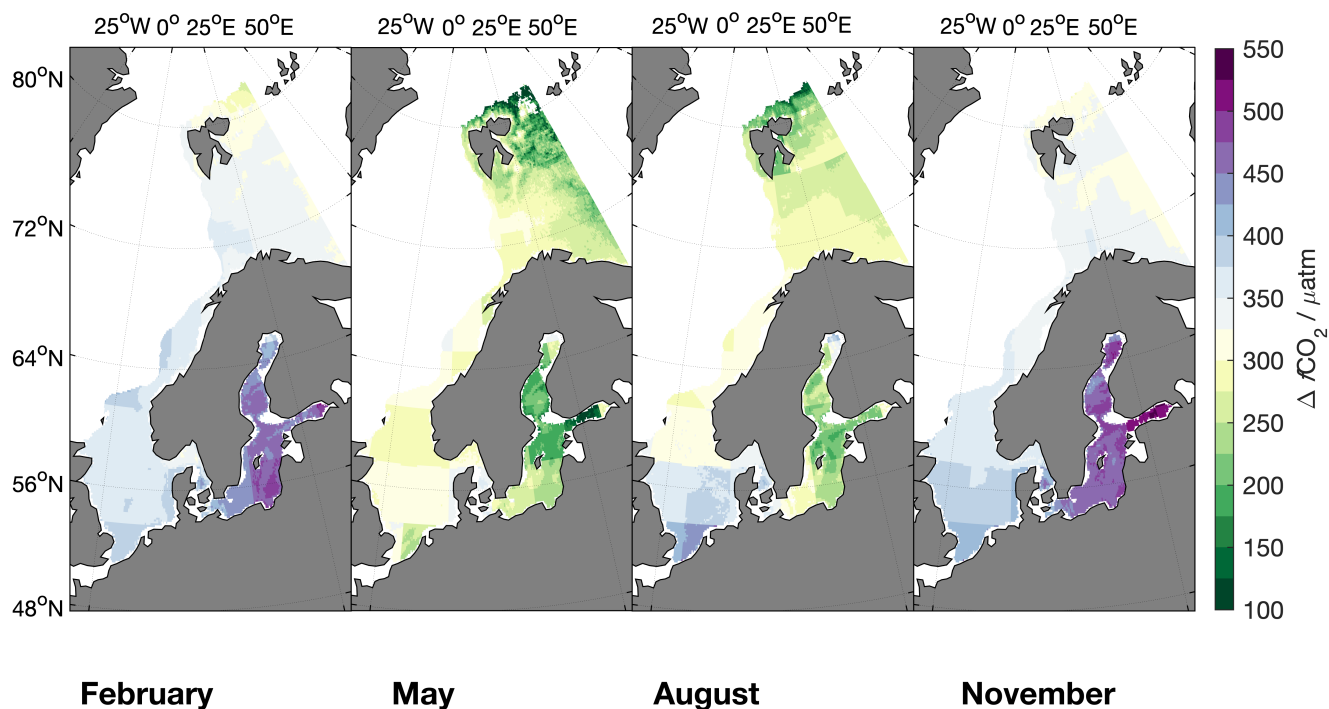
Figure 4. The average fCO$_2$ of MLR 1 (1998-2016) for one example months in each season (February, May, August and November).

et al., 2015). In the North Sea, the pH is in the same range as reported in Salt et al. (2013) and it also shows the same distribution in August/September with higher pH in the northern North Sea and lower pH in the southern part.

4 Discussion

4.1 Validation of the pCO$_2$ maps

5   The performance of the MLR and the produced maps are evaluated in different ways: (1) the R^2 and the RMSE of the fit between the driver data and the gridded observations, (2) the average deviation and its standard deviation, as well as the ME between the produced fCO$_2$ maps and the gridded observations as a regional average, (3) showing the median deviation between the MLR and the gridded observations on a monthly level, (4) by comparing the data from the fCO$_2$ maps to observations from two time series stations. (2) - (4) will be shown for both, the time period covered by the driver data (1998-2016) and a prediction of the

10   maps into the years 2017 and 2018. Please note that the comparability of the model performance between the different regions
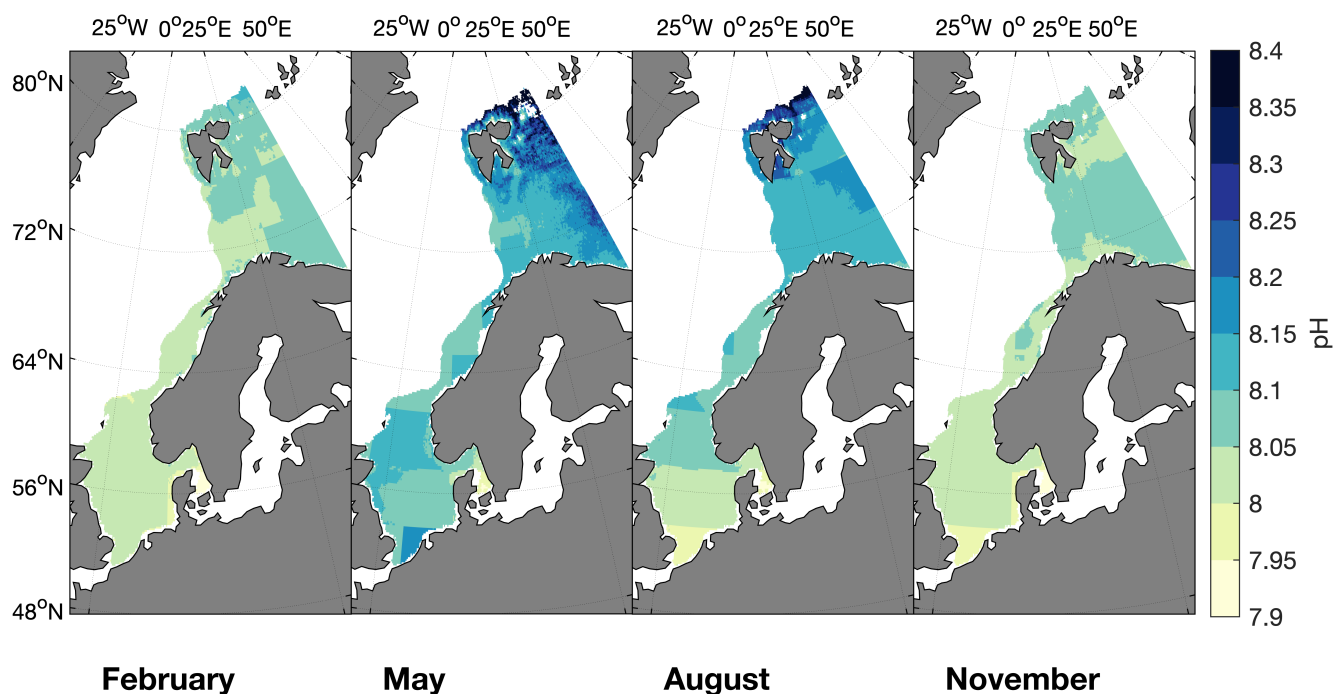
Figure 5. The average pH based on MLR 1 (1998-2016) for one example month in each season (February, May, August and November).

is limited. All used statistical parameters are influenced by characteristics that can vary substantially between the different regions, such as range of the data, their variability or the amount of grid cells with data. Additionally, in a region with many measurements the amount of variability captured by these measurements is most likely larger and, thus will lead to a weaker correlation.

5   Generally, the uncertainty of MLR 1 are in the same range as in other studies (Laruelle et al., 2017; Yasunaka et al., 2018) mapping coastal $f\mathrm{CO_2}$ dynamics: 25 μatm in the North Sea, 16 μatm along the Norwegian Coast, 12 μatm in the Barents Sea, and 39 μatm in the Baltic Sea (based on the RMSE in Table 5). In the Baltic Sea, which has a large variability in itself, Parard et al. (2016) obtained lower standard deviations through dividing the area in smaller sub-regions.

The seasonal differences between MLR 1 and the SOCAT v5 data for each region are shown in Figure 6. This comparison
10   shows a very good agreement. For MLR 1, the seasonal variations of the median bias are small in the North Sea, along the Norwegian coast and in the Baltic Sea. In the Barents Sea, however, the bias varies seasonally. Here, MLR 1 slightly underestimates the $f\mathrm{CO_2}$ in winter and early spring, while it overestimates the $f\mathrm{CO_2}$ in summer. In all other regions, the
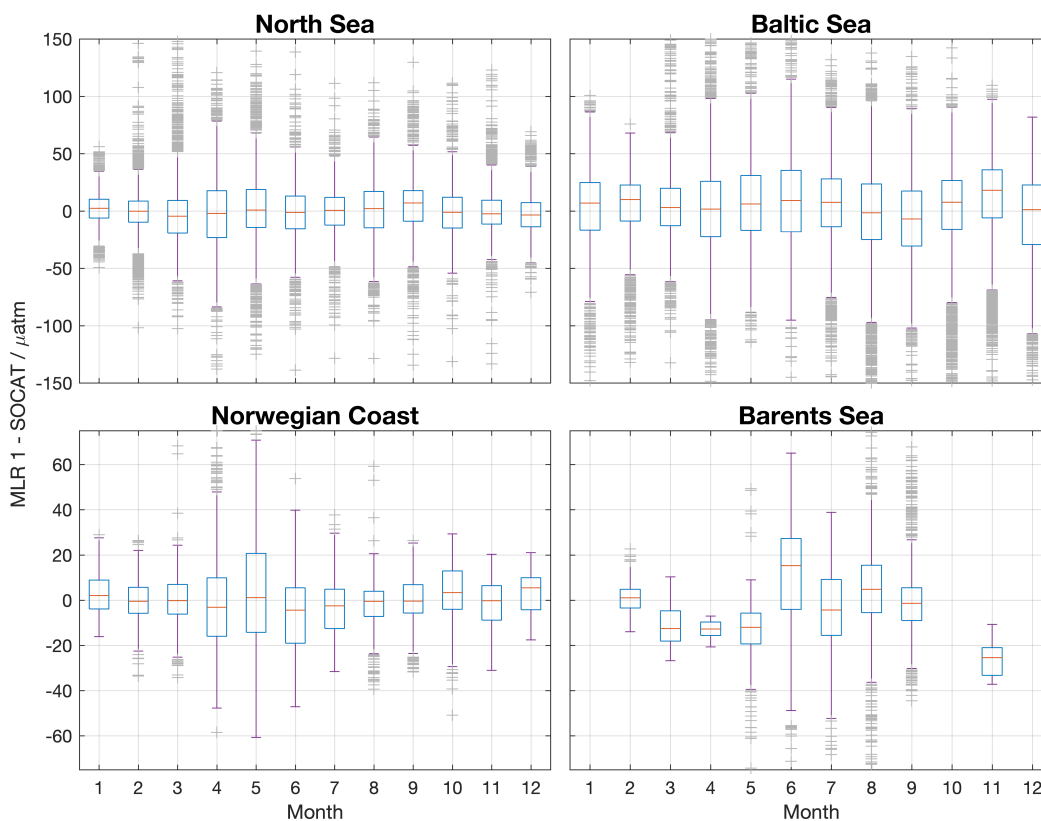
Figure 6. Boxplots showing the median deviation of MLR 1 from the gridded SOCAT v5 data for each region (red line). The boxes show the respective 75% percentiles. 99% of the data lays within the range of the purple whiskers. Extremes are shown as gray crosses.

median seasonal bias is smaller than the uncertainty of the maps. The larger seasonal bias in the Barents sea is most likely caused by the larger seasonal bias in the number of available observations. There is no data available in October, December and January.

When comparing all observations from the years 2017 and 2018 to the predictions by the MLR1, we find a good agreement in the North Sea (2 ± 20 μatm) and no seasonal bias (Figure 7). In the other regions, the agreement is somewhat reduced compared to the years 1998-2016 (-9 ± 39 μatm (Norwegian Coast), -5 ± 29 μatm (Barents Sea) and 28 ± 58 μatm (Baltic Sea)). In these regions we also observe a seasonal bias in the years 2017 and 2018. At least for the Baltic Sea this could be a reason of a extraordinarily warm and dry summer in 2018, that lead to very low fCO$_2$ values in the Baltic Sea Bakker et al. (2016) Please note that for this comparison, the MLR was extrapolated in time. Only observations until December 2016 were used to produce the MLR.

In a second test to investigate to which extent MLR 1 can reproduce observations we compared the MLR output with time series data from two voluntary observing ship lines in two very different regions with a good data coverage: M/V Nuka Arctica
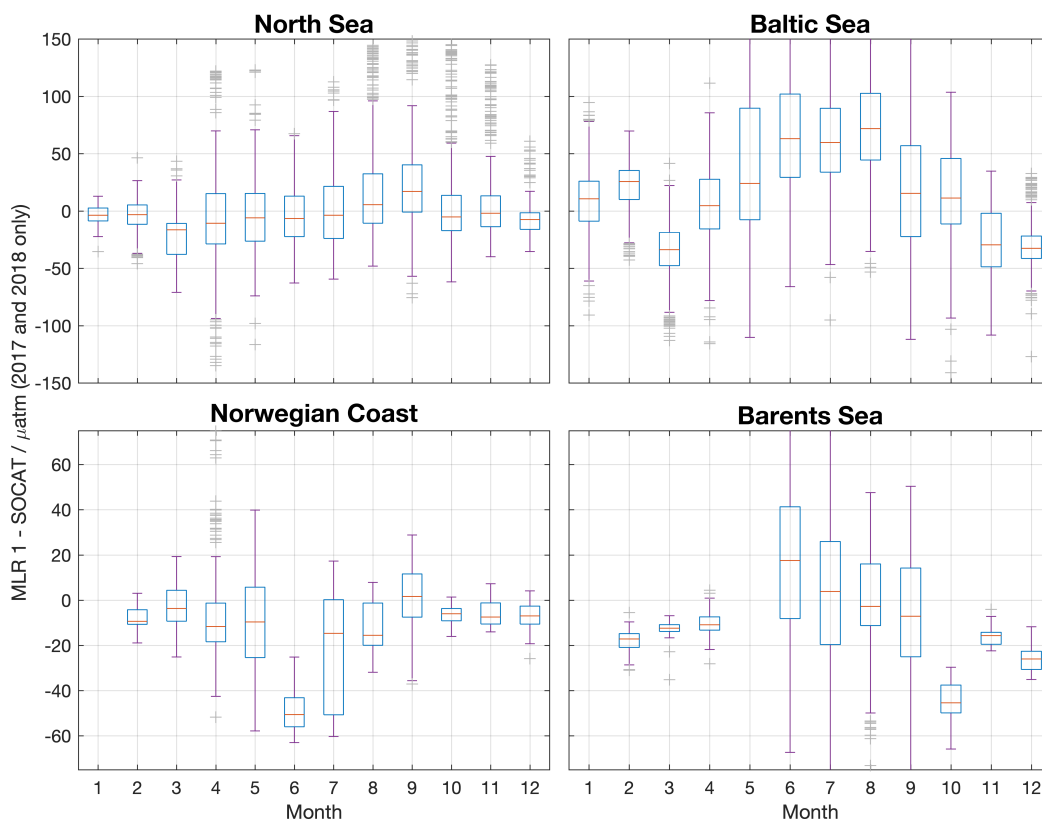
Figure 7. Boxplots showing the median deviation of MLR 1 (based on observations until 2016) predicted and measured $f\mathrm{CO_2}$ values in 2017 and 2018. The boxes show the respective 75% percentiles. 99% of the data lays within the range of the purple whiskers. Extremes are shown as gray crosses. The number of grid cells with data available were: North Sea: 5047 , Norwegian Coast: 1543, Barents Sea: 2312, Baltic Sea: 5414.

in the northern North Sea (0-2°E, 58-60°N) and M/V Finnmaid in the Baltic Sea (23-24°E, 59-60°N) (Figure 8). To every observation we assigned the related value of MLR 1. The agreement between the MLR 1 and the observations is very good. MLR 1 reproduces the general seasonality and some of the interannual variability, also in the years 2017 and 2018, of which the observations were not used in the regression.

5   When performing interpolation exercises it is always important to be aware of the fact that the resulting maps might come with biases and do not represent all regions equally well. While the here presented maps give a good general overview about the surface ocean $f\mathrm{CO_2}$ variability in regions with a relatively large amount of data, the reliability, however, is limited in those regions where the data coverage is more scarce. This is especially the case, when the region with scarce data coverage is showing different characteristics in, for example, temperature and salinity, compared to the rest of the region. One such

10   example is the Gulf of Bothnia in the Baltic Sea region where almost all data used to derive the MLR is from south of 60°N
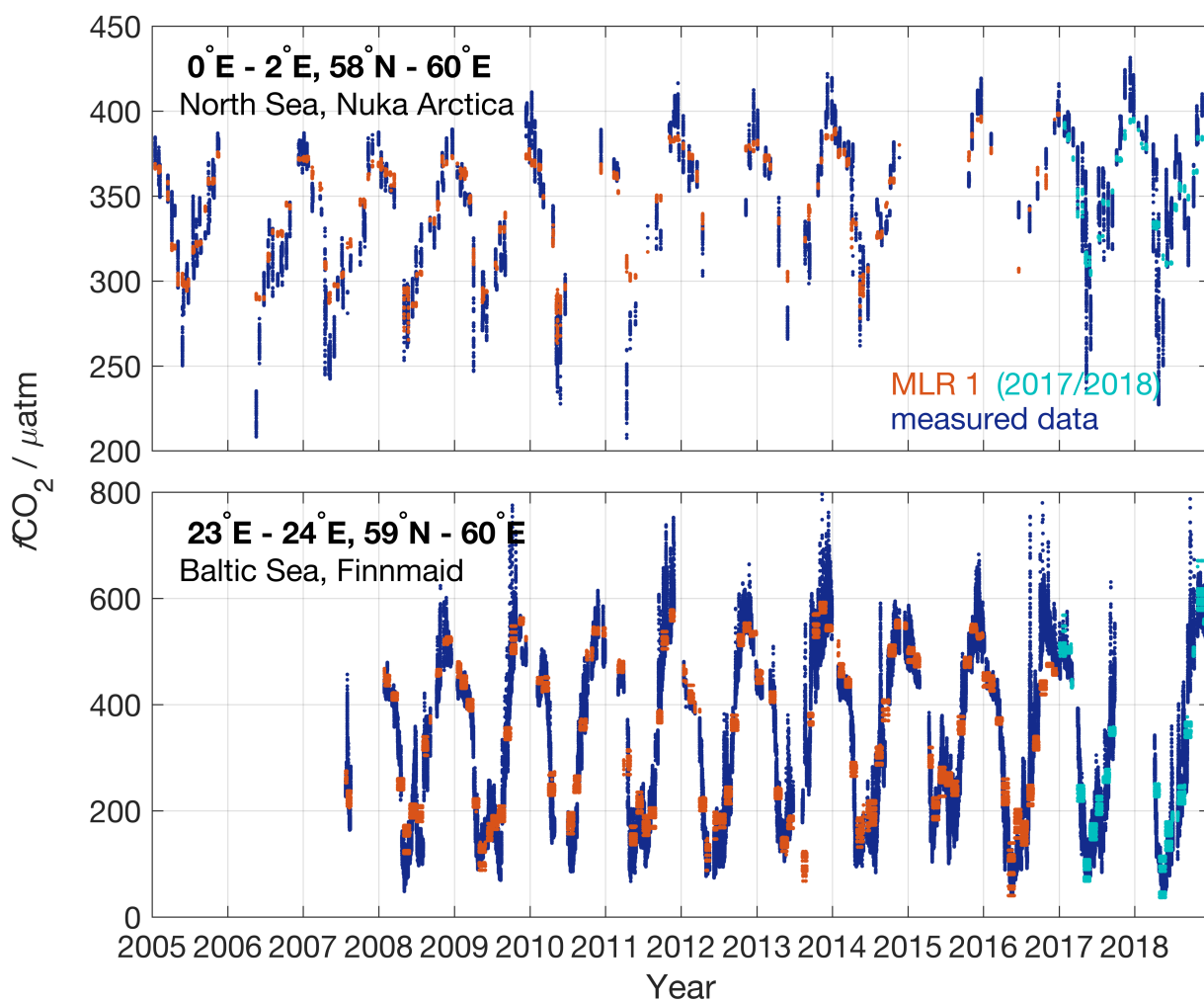
Figure 8. Time series of VOS data from Nuka Arctica (upper panel, blue) and Finnmaid (lower panel, blue) compared with MLR 1 at the same location (red). In light blue the predictive MLR output for the years 2017 and 2018 is shown.

i.e. not in the Gulf of Bothnia, but in the Baltic Proper and western Baltic Sea (Figure 2). The MLR method can also lead to unrealistic extreme values and even negative $f\mathrm{CO_2}$. Some such values occur in the northeastern Barents sea as well as in some parts of the Baltic Sea (about 0.01% of the grid cells in each region). As pH cannot be calculated for negative $f\mathrm{CO_2}$, we excluded all negative $f\mathrm{CO_2}$ values for the calculation of pH. Excluding the negative values resulted in a change of the average

5 $f\mathrm{CO_2}$ of 0.05 μatm (Baltic Sea) and 0.3 μatm (Barents Sea) so they are of negligible importance for the flux estimates. While the negative values are easy to spot and discard there are most likely more unrealistically low values in spring and summer data in the very north and northeastern Barents Sea as well as some parts of the Baltic Sea. However, there are no data available in SOCAT v5 or elsewhere available to validate this to validate this.

All regions with questionable $f\mathrm{CO_2}$ are also questionable in their pH data. There is a number of very high pH in the Barents

10 Sea, that are associated with also very low $f\mathrm{CO_2}$ that might not be realistic. In addition, estimated pH values in regions or seasons where the actual alkalinity-salinity deviates strongly from the Nondal et al. (2009) one used here, should be interpreted with caution.

4.2 Trends in $f\mathrm{CO_2}$ and pH

The trends in surface ocean $f\mathrm{CO_2}$ in coastal regions are often difficult to assess because of the scarcity of the data relative to the

15 highly dynamical character of these regimes and their large interannual variability. One issue is that the start of the productive season can range from February to April even within a small area, such that even restricting the analysis to specific seasons (e.g. winter) can be challenging. However, due to lack of data, especially winter data, most observational studies are based on repeated sections during summer. Further, the fact that these measurements typically do not take place every year, adds even more uncertainty to the estimated trend, as the interannual variability can mask the trend signal.

20 The monthly maps of $f\mathrm{CO_2}$ from 1998 to 2016 enable us now to estimate the trend in surface ocean $f\mathrm{CO_2}$ for the entire region and equally distributed over the seasons (Figure 9, left). All trends were computed by using deseasonalized data. The interannual variability of the trend estimates in each region is shown in the panels on the right hand side in Figure 9. Based on the linear regression the significant trends in $f\mathrm{CO_2}$ have an average uncertainty of 0.5 μatm/yr (North Sea), 0.4 μatm/yr (Norwegian Coast), 0.4 μatm/yr (Barents Sea), and 0.7 μatm/yr (Baltic Sea), while the shorter time periods shown have a

25 higher and the longer time periods a lower uncertainty. For pH trends the average uncertainty of the regression is $5 \cdot 10^{-4}$ (North Sea) and $7 \cdot 10^{-4}$ (Norwegian Coast and Barents Sea).

In most of the regions addressed in this study, the trend in the surface ocean is lower than the trend in atmospheric $x\mathrm{CO_2}$ (global average 2.02 ppm yr^{-1} ("Cooperative Global Atmospheric Data Integration Project", 2015)). Trends exceeding the atmospheric values in the period from 1998 to 2016 can only be observed at the entrance of the English Channel, in Storfjor-

30 den/Svalbard, the Gulf of Finland and the Gulf of Bothnia ($2.5 - 3$ μatm yr^{-1}). It has to be noted that there was almost no measured $f\mathrm{CO_2}$ as MLR input in neither Storfjorden nor the Gulf of Bothnia. Therefore, these trends should be handled with care. The western North Sea has a trend that is only slightly lower than the trend in the atmosphere ($1.5 - 2$ μatm yr^{-1}), while the trends in the eastern North Sea, along the Norwegian coast and in the Barents Sea are somewhat lower (0.5-1.5 μatm yr^{-1}). In the North Sea this is consistent with a recent study directly based on observations Omar et al. (2019). The low trends result
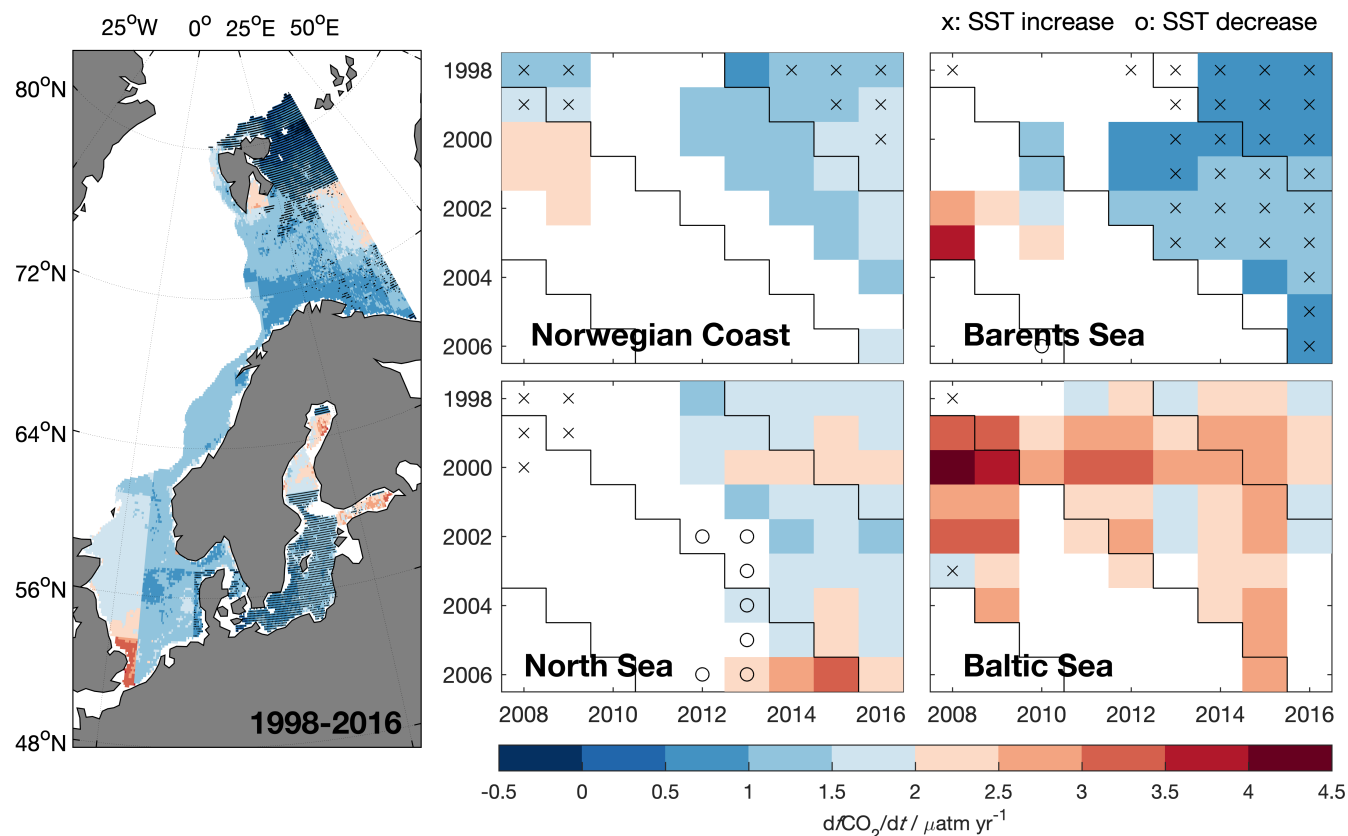
Figure 9. The trend in surface ocean $f\mathrm{CO}_2$ estimated from deseasonalized $f\mathrm{CO}_2$. The left hand panel show the spatial distribution of the trend over the time period from 1998 to 2016. Grid boxes without a significant trend are denoted with a black dot. On the right hand the influence of the time range on the average trend is shown for the four regions. Non significant trends were left blank. Significant trends in sea surface temperature are indicated with crosses/circles.

in an increase in the strength of the ocean carbon sink with time. A trend smaller than the atmospheric trend can be caused by a shift in the bloom onset. For example, in the North Sea a significant drawdown in $f\mathrm{CO}_2$ has been observed as early as February in some years (Omar et al., 2019). The bloom onset in the North Sea after the 1990s has been shown to be mainly triggered by the spring-neap tidal cycle and the air temperature by Sharples et al. (2006). They found that the onset of spring

5   bloom has occurred on average 1 day earlier every year. Over the period covered in this study (almost 20 years) this could cause a change of three weeks in the timing of the spring bloom. Even if the trend in winter $f\mathrm{CO}_2$ was following the atmospheric $x\mathrm{CO}_2$ increase, such a change in bloom onset would lead to a trend lower than the atmospheric when averaging over the entire year.
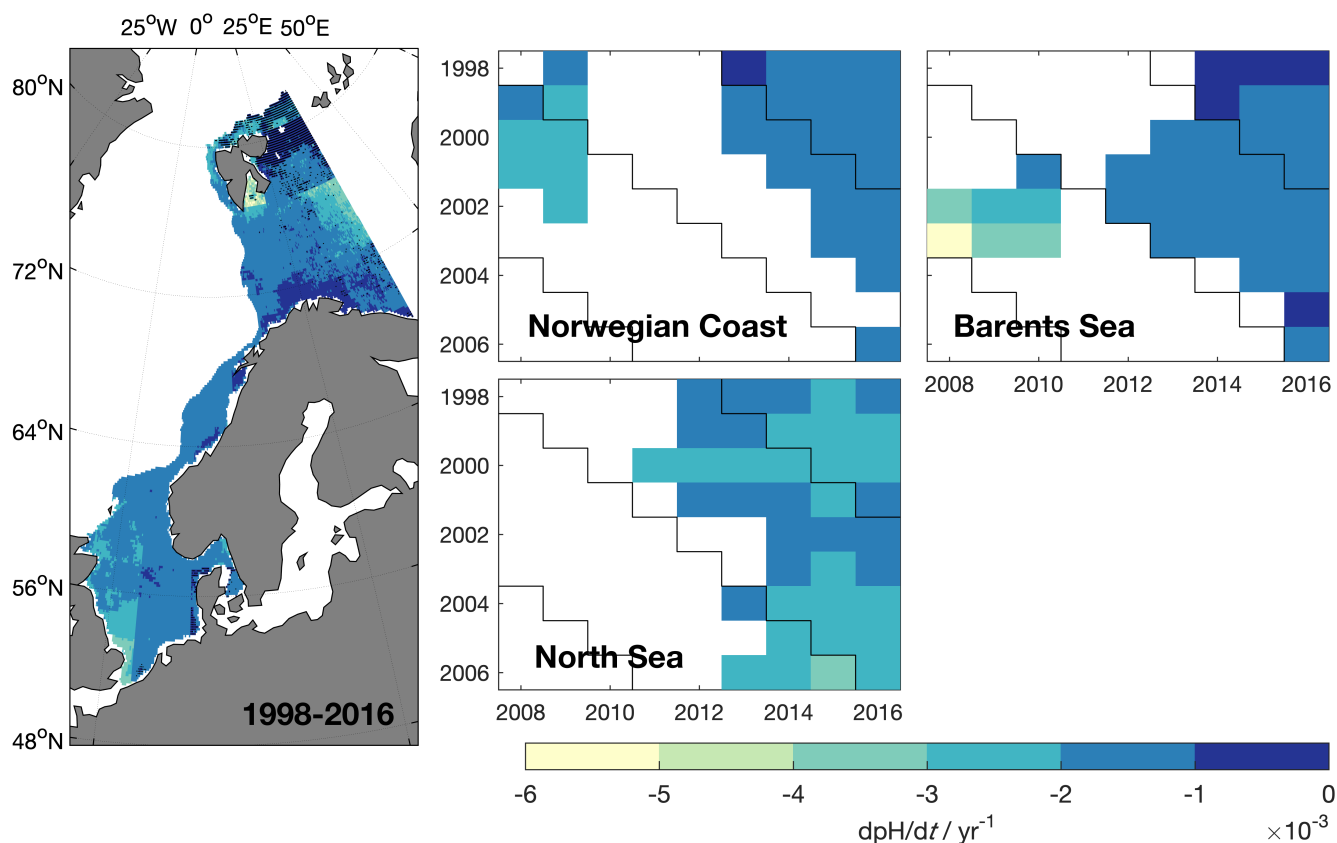
Figure 10. The trend in surface ocean pH estimated from deseasonalized pH. On the left hand the spatial distribution of the trend over the time period from 1998 to 2016 is shown. Grid boxes without a significant trend are denoted with a black dot. On the right hand the influence of the time range on the average trend is shown for the four regions. Non significant trends were left blank.

The observation that large subareas (the Baltic Sea, the western North Sea) did not show a significant trend can be explained by the fact that, coastal systems, especially enclosed areas as the Baltic Sea, experience a high anthropogenic pressure. Anthropogenic impacts other than rising atmospheric CO_2 concentrations influencing the ocean carbon system and the bloom properties such as the nutrient load of rivers can effect coastal ecosystems through eutrification, resulting in lower fCO_2 in
5   summer and higher fCO_2 in winter. Another important process that influences the carbon system in the Baltic Sea are inflow events from the North sea. In between such events, CO_2 accumulates in deeper water layers causing an increasing gradient of dissolved inorganic carbon (DIC) across the halocline. Whenever deep winter mixing occurs, this will then lead to a large increase of surface fCO_2 because of the input of DIC rich waters from below. Another reason is the observed change in alkalinity with time which effects the fCO_2 though changes in the buffer capacity of the inorganic carbon system (Müller et al.,
10   2016).

When looking at the interannual variability, it becomes obvious that the trend in the North Sea is slightly smaller than the atmospheric CO_2 trend. In contrast, the Norwegian coast and the Barents Sea experience a robust trend much lower than the atmospheric trend (Norwegian Coast: $1 - 1.5$ μatm yr^{-1}, Barents Sea: around 1 μatm yr^{-1}). Here we can also see a stable pattern of warming over time scales of 10 to 15 years. The warming in itself would result in an increase of $f CO_2$ with time, in addition to the atmospheric forcing. As we are observing a trend smaller than the atmospheric trend, temperature effects can't be the driver here. The lower trend stems most likely from an earlier onset of spring bloom. It has been shown that the atlantification and the reduced ice coverage of the Barents sea leads to a longer productive season, and this will result in more months with strong undersaturation in CO_2 (Oziel et al., 2016). In the Baltic Sea the pattens are different. Here the variability is much larger, while most of the time periods show a trend larger than the atmospheric trend ($3 - 3.5$ μatm yr^{-1}). Although slightly smaller our results broadly agree with trend estimates based on measurements of 4.6 - 6.1 μatm yr^{-1} over 2008-2015 (Schneider and Müller, 2018). Finally, it also needs to be noted that the uncertainty of the $f CO_2$ maps was highest in the Baltic Sea. This makes it also more difficult, if not impossible, to properly detect these small trends.

For pH, the trend in most regions is around -0.002 yr^{-1} (Figure 10). A expected, regions with the strongest trend in $f CO_2$ also show the highest trend in pH, such as the southern North Sea. The trend in the northern North Sea and along the Norwegian Coast is in good agreement with the pH trends found in studies focusing on the open Atlantic Ocean (-0.0022 yr^{-1} (Lauvset and Gruber, 2014)) and the North Atlantic and Nordic Seas (-0.002 yr^{-1} (Lauvset et al., 2015)).

4.3 CO$_2$ disequilibrium and flux

The average sea-air CO_2 disequilibrium ($\Delta f CO_2 = f CO_{2,\text{sea}} - f CO_{2,\text{atm}}$) is shown in Figure 11. The only region showing an average supersaturation is the southern North Sea. Towards the north, the surface ocean becomes more and more undersaturated, with lowest values in the Barents Sea. The values we found in the Barents Sea (-60 to -80 μatm in the southern Barents Sea and less than -100 μatm around Svalbard) are in generally in agreement those estimated by Yasunaka et al. (2018). The seasonal cycle of $\Delta f CO_2$ follows a mainly biologically driven pattern with higher values in the winter and lower values from April to August. The seasonal cycle is largest in the Baltic and smallest in the Barents Sea.

The sea-air CO_2 fluxes (Figure 12) show that most regions are a net and increasing sink for CO_2. The only source net regions are the southern North Sea and the Baltic Sea. The two different regimes in the North Sea with the southern, nonstratified part being a source and the northern temporarily stratified part a sink for CO_2, are well described in the literature (Thomas et al., 2004).

The seasonal variations in the air-sea flux are driven by a combination of the changes in the disequilibrium, the wind strength, and the ice cover. As there is less wind during summer, when the disequilibrium is large, but a smaller disequilibrium during winter, when the wind strength is high, the seasonal variability is often less clear than that of e.g. the disequilibrium. This can be seen in the Barents Sea and Norwegian Coast. Yasunaka et al. (2018) found the seasonal and interannual variation in the Barents Sea and the Norwegian Sea mostly corresponded to the wind speed and the sea ice concentration. In contrast to that we see the strongest dependence on the air-sea disequilibrium. However, even though we don't find the same seasonality, considering the error margin and the small amplitude of the seasonality, our average fluxes fit well with those reported by
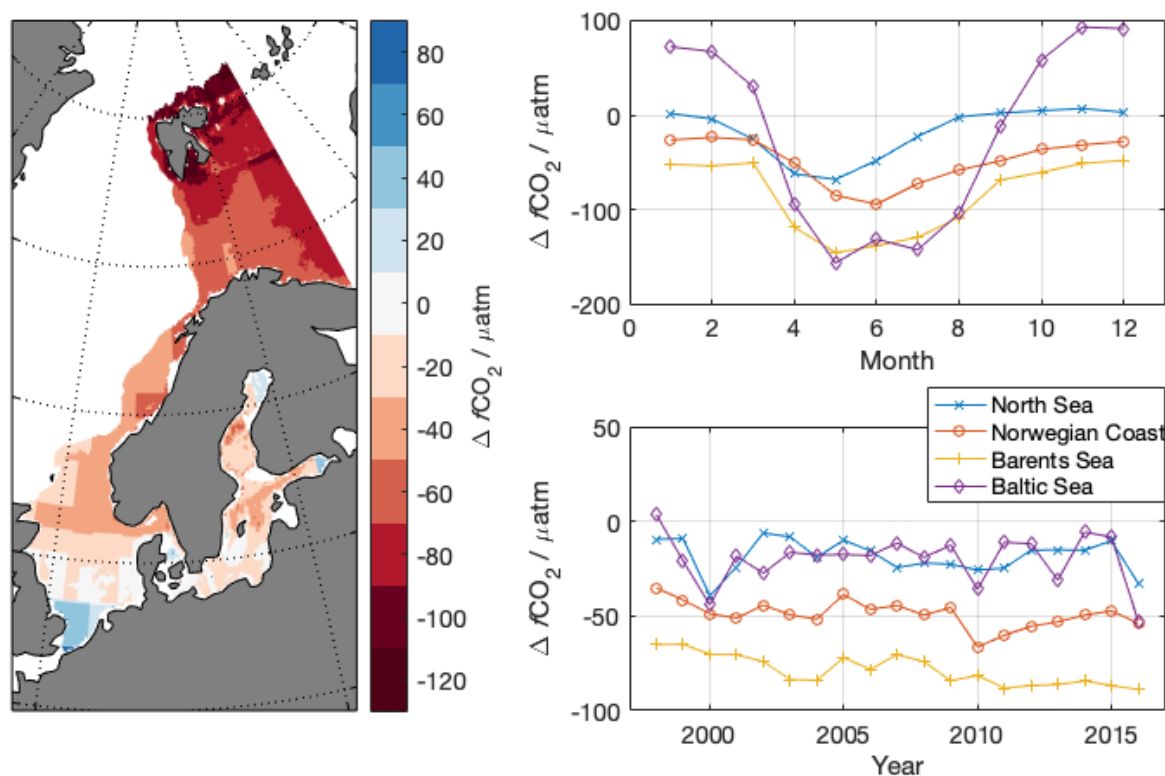
Figure 11. The average air-sea CO_2 disequilibrium over the period 1998-2016 (left hand panel, red colors indicate average undersaturation, while blue colors indicate average oversaturation). For every region average disequilibria are shown as seasonal averages (right side, upper corner) and time-series of annual disequilibria (right side, lower corner). Blue line: North Sea, red line: Norwegian coast, yellow line: Barents Sea, purple line: Baltic Sea

Yasunaka et al. (2018) of -8 to -12 mmol m^{-2} d^{-1} (Barents Sea) and -4 to -8 mmol m^{-2} d^{-1} (Norwegian Coast). In the North Sea there is almost no net flux during winter, as the surface ocean is more or less in equilibrium with the atmosphere. In the Baltic Sea, we can see high fluxes into the atmosphere during winter as here a large oversaturation coincides with high wind strengths. This is also why the Baltic Sea is a net source regions. Although Parard et al. (2017) did find slightly smaller fluxes (+15 mmol m^{-2} d^{-1} during winter and -8 mmol m^{-2} d^{-1} during summer), the annual air-sea CO_2 fluxes are in good agreement (0 to +4 mmol m^{-2} d^{-1} between 1998 and 2011).

The uncertainty in the calculated fluxes is a result of the uncertainties in the fCO_2 observations, ΔfCO_2 maps, the gas exchange parameterization and the wind product. The uncertainty of the ΔfCO_2 is mostly driven by the uncertainty of the MLR, resulting in an error between 12 μatm and 39μatm, according to the RMSE values of MLR1 for the different regions (Table 5). A number of studies addresses on the uncertainty of gas exchange parameterizations and the wind products (Couldrey et al., 2016; Gregg et al., 2014; Ho and Wanninkhof, 2016). For this study, we apply an uncertainty of the gas transfer velocity
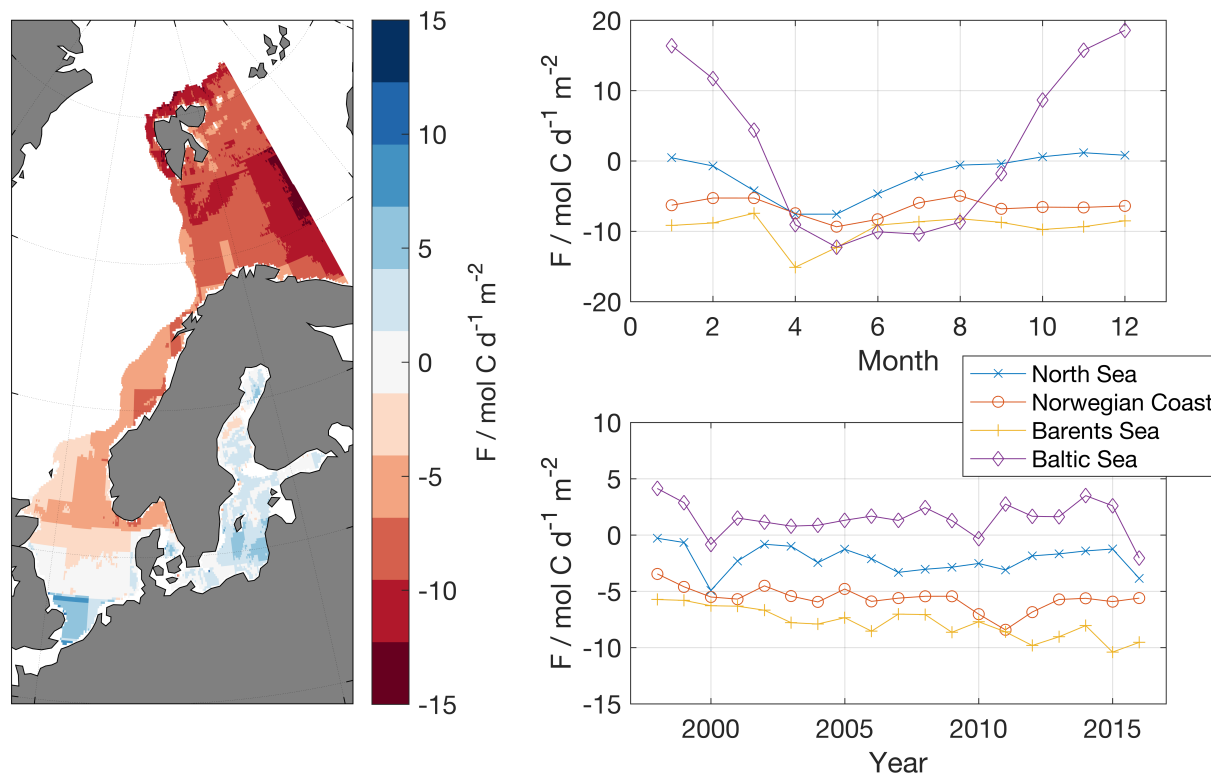
Figure 12. The average air-sea CO_2 flux over the period 1998-2016 (left hand panel, red colors indicate sink regions, while blue colors indicate source regions). For every region average fluxes are show as seasonal averages (right side, upper corner) and timeseries of annual fluxes (right side, lower corner).

of 20% (Wanninkhof, 2014). This will result in an uncertainty of the air-sea flux of about 2 mmol C d^{-1} m^{-2}. It has to be kept in mind, that the absolute uncertainty in k increases with increasing wind speed, but that the uncertainty in the wind speed has largest influence in summer when also the disequilibrium is large. In contrast to that the uncertainty in $\Delta f CO_2$ will cause larger errors in winter, when the wind speeds are high.

5 Conclusions

The MLR approach presented in this work is a relatively easy and straight forward method to produce monthly $f CO_2$ maps with a high spatial resolution in coastal regions. Using available open ocean maps did improve the coastal maps significantly. The maps reproduce nicely the main spatial and temporal patterns that can also be found in observations in the different regions for both $f CO_2$ and pH. The surface seawater $f CO_2$ trends were mostly lower than the atmospheric trends and also lower than the trends found in the open North Atlantic. We did find the northern European shelf to be an increasing net sink for CO_2. Only

the Baltic Sea is a net source region. This method clearly has the potential to be extended to a larger region. However, it should be handled with care in regions with only a small number of observations as the MLR can lead to unrealistic values.

Longterm observations with a high temporal resolution are extremely important for developing maps such as presented here. While a decent spatial coverage exists for the open North Atlantic, most coastal regions are still undersampled. This is in particular the case for higher latitudes and in the Arctic. To further understand and interpret the trends on $f\mathrm{CO}_2$ and pH it is necessary to increase our knowledge and understanding of the interaction of primary production, respiration in the water column and the sediments, mixing and gas exchange and their influence on the carbon cycle.

While MLR derived sea surface provides coherent picture of the entire region, they have clear limitations and should be interpreted with caution in regions with few or none observations. Both, for producing high quality maps, as well for their validation a large number of observations is essential.Also, observations of second parameter of the carbon system would be beneficial for deriving pH maps. This will help to reduce and quantify the error introduced by estimating alkalinity from salinity. In addition to that, our work neglects the areas closest to land due to unavailability of CO_2 data and reanalysis products in those areas. For adding their contribution to the flux estimates, new platforms specialized on measurements directly at the land-ocean interface need to be developed.

Data availability. The dataset is available under: https://doi.org/10.18160/939X-PMHU.

Competing interests. The authors declare no competing interests.

Acknowledgements. First of all, we want to thank everyone involved in the collection and quality control of surface ocean CO_2 data. The Surface Ocean CO_2 Atlas (SOCAT) is an international effort, endorsed by the International Ocean Carbon Coordination Project (IOCCP), the Surface Ocean Lower Atmosphere Study (SOLAS) and the Integrated Marine Biosphere Research (IMBeR) program, to deliver a uniformly quality-controlled surface ocean CO_2 database. The many researchers and funding agencies responsible for the collection of data and quality control are thanked for their contributions to SOCAT. We used NCEP Reanalysis 2 data provided by the NOAA/OAR/ESRL PSD, Boulder, Colorado, USA, from their web site at https://www.esrl.noaa.gov/psd/. This study has been conducted using E.U. Copernicus Marine Service Information. This work was funded by the project ICOS Norway (Research Council of Norway, 245927). This project has received funding from the European Union's Horizon 2020 research and innovation program under grant agreement No 776810. This work was supported by BONUS INTEGRAL, receiving funding from BONUS (Art 185) by the EU and the contributing national funding agencies, Grant No. 03F0773A of the German Ministry for Education and Research.

References

Bakker, D. C. E., Pfeil, B., Landa, C. S., Metzl, N., O'Brien, K. M., Olsen, A., Smith, K., Cosca, C., Harasawa, S., Jones, S. D., Nakaoka, S.-i., Nojiri, Y., Schuster, U., Steinhoff, T., Sweeney, C., Takahashi, T., Tilbrook, B., Wada, C., Wanninkhof, R., Alin, S. R., Balestrini, C. F., Barbero, L., Bates, N. R., Bianchi, A. A., Bonou, F., Boutin, J., Bozec, Y., Burger, E. F., Cai, W.-J., Castle, R. D., Chen, L.,

5   Chierici, M., Currie, K., Evans, W., Featherstone, C., Feely, R. A., Fransson, A., Goyet, C., Greenwood, N., Gregor, L., Hankin, S., Hardman-Mountford, N. J., Harlay, J., Hauck, J., Hoppema, M., Humphreys, M. P., Hunt, C. W., Huss, B., Ibánhez, J. S. P., Johannessen, T., Keeling, R., Kitidis, V., Körtzinger, A., Kozyr, A., Krasakopoulou, E., Kuwata, A., Landschützer, P., Lauvset, S. K., Lefèvre, N., Monaco, C. L., Manke, A., Mathis, J. T., Merlivat, L., Millero, F. J., Monteiro, P. M. S., Munro, D. R., Murata, A., Newberger, T., Omar, A. M., Ono, T., Paterson, K., Pearce, D., Pierrot, D., Robbins, L. L., Saito, S., Salisbury, J., Schlitzer, R., Schneider, B., Schweitzer,

10   R., Sieger, R., Skjelvan, I., Sullivan, K. F., Sutherland, S. C., Sutton, A. J., Tadokoro, K., Telszewski, M., Tuma, M., Heuven, S. M. A. C. v., Vandemark, D., Ward, B., Watson, A. J., and Xu, S.: A multi-decade record of high-quality fCO$_2$ data in version 3 of the Surface Ocean CO$_2$ Atlas (SOCAT), Earth System Science Data, 8, 383–413, https://doi.org/https://doi.org/10.5194/essd-8-383-2016, https://www.earth-syst-sci-data.net/8/383/2016/, 2016.

Bauer, J. E., Cai, W.-J., Raymond, P. A., Bianchi, T. S., Hopkinson, C. S., and Regnier, P. A. G.: The changing carbon cycle of the coastal

15   ocean, Nature, 504, 61–70, https://doi.org/10.1038/nature12857, https://www.nature.com/articles/nature12857, 2013.

Bourgeois, T., Orr, J. C., Resplandy, L., Terhaar, J., Ethé, C., Gehlen, M., and Bopp, L.: Coastal-ocean uptake of anthropogenic carbon, Biogeosciences, 13, 4167–4185, https://doi.org/https://doi.org/10.5194/bg-13-4167-2016, https://www.biogeosciences.net/13/4167/2016/, 2016.

Bricheno, L. M., Wolf, J. M., and Brown, J. M.: Impacts of high resolution model downscaling in coastal regions, Continental Shelf Research,

20   87, 7–16, https://doi.org/10.1016/j.csr.2013.11.007, http://www.sciencedirect.com/science/article/pii/S0278434313003725, 2014.

Cavalieri, D. J., Parkinson, C. L., Gloersen, P., and Zwally, H. J.: Sea Ice Concentrations from Nimbus-7 SMMR and DMSP SSM/I-SSMIS Passive Microwave Data, Version 1, Monthly, doi:https://doi.org/10.5067/8GQ8LZQVL0VL, 1996.

Center, N. G. D.: 2-minute Gridded Global Relief Data (ETOPO2) v2, NOAA, https://doi.org/doi:10.7289/V5J1012Q, 2006.

"Cooperative Global Atmospheric Data Integration Project": Multi-laboratory compilation of atmospheric carbon dioxide data for the period

25   1968-2014, obspack_co2_1_GLOBALVIEWplus_v1.0_2015-07-30, https://doi.org/10.15138/G3RP42, published: NOAA Earth System Research Laboratory, Global Monitoring Division, 2015.

Couldrey, M. P., Oliver, K. I. C., Yool, A., Halloran, P. R., and Achterberg, E. P.: On which timescales do gas transfer velocities control North Atlantic CO2 flux variability?, Global Biogeochemical Cycles, 30, 787–802, https://doi.org/10.1002/2015GB005267, https://agupubs.onlinelibrary.wiley.com/doi/abs/10.1002/2015GB005267, 2016.

30   Dickson, A. and Millero, F.: A comparison of the equilibrium constants for the dissociation of carbonic acid in seawater media, Deep-Sea Res. Pt I, 34, 1733 – 1743, https://doi.org/10.1016/0198-0149(87)90021-5, 1987.

Dickson, A. G.: Standard potential of the reaction: AgCl(s) + 12H2(g) = Ag(s) + HCl(aq), and and the standard acidity constant of the ion HSO4 in synthetic sea water from 273.15 to 318.15 K, The Journal of Chemical Thermodynamics, 22, 113–127, https://doi.org/10.1016/0021-9614(90)90074-Z, http://www.sciencedirect.com/science/article/pii/002196149090074Z, 1990.

35   Fay, A. R. and McKinley, G. A.: Correlations of surface ocean pCO2 to satellite chlorophyll on monthly to interannual timescales, Global Biogeochemical Cycles, 31, 436–455, https://doi.org/10.1002/2016GB005563, https://agupubs.onlinelibrary.wiley.com/doi/abs/10.1002/2016GB005563, 2017.

Fröb, F., Olsen, A., Becker, M., Chafik, L., Johannessen, T., Reverdin, G., and Omar, A.: Wintertime fCO2 Variability in the Subpolar North Atlantic Since 2004, Geophysical Research Letters, 46, 1580–1590, https://doi.org/10.1029/2018GL080554, https://agupubs.onlinelibrary.wiley.com/doi/abs/10.1029/2018GL080554, 2019.

Gregg, W. W., Casey, N. W., and Rousseaux, C. S.: Sensitivity of simulated global ocean carbon flux estimates to forcing by reanalysis products, Ocean Modelling, 80, 24–35, https://doi.org/10.1016/j.ocemod.2014.05.002, http://www.sciencedirect.com/science/article/pii/S1463500314000651, 2014.

Griffiths, J. R., Kadin, M., Nascimento, F. J. A., Tamelander, T., Törnroos, A., Bonaglia, S., Bonsdorff, E., Brüchert, V., Gårdmark, A., Järnström, M., Kotta, J., Lindegren, M., Nordström, M. C., Norkko, A., Olsson, J., Weigel, B., Žydelis, R., Blenckner, T., Niiranen, S., and Winder, M.: The importance of benthic–pelagic coupling for marine ecosystem functioning in a changing world, Global Change Biology, 23, 2179–2196, https://doi.org/10.1111/gcb.13642, https://onlinelibrary.wiley.com/doi/abs/10.1111/gcb.13642, 2017.

Gruber, N., Clement, D., Carter, B. R., Feely, R. A., Heuven, S. v., Hoppema, M., Ishii, M., Key, R. M., Kozyr, A., Lauvset, S. K., Monaco, C. L., Mathis, J. T., Murata, A., Olsen, A., Perez, F. F., Sabine, C. L., Tanhua, T., and Wanninkhof, R.: The oceanic sink for anthropogenic CO2 from 1994 to 2007, Science, 363, 1193–1199, https://doi.org/10.1126/science.aau5153, http://science.sciencemag.org/content/363/6432/1193, 2019.

Ho, D. T. and Wanninkhof, R.: Air–sea gas exchange in the North Atlantic: 3He/SF6 experiment during GasEx-98, Tellus B: Chemical and Physical Meteorology, 68, 30 198, https://doi.org/10.3402/tellusb.v68.30198, https://doi.org/10.3402/tellusb.v68.30198, 2016.

Jones, S. D., Quéré, C. L., Rödenbeck, C., Manning, A. C., and Olsen, A.: A statistical gap-filling method to interpolate global monthly surface ocean carbon dioxide data, Journal of Advances in Modeling Earth Systems, 7, 1554–1575, https://doi.org/10.1002/2014MS000416, https://agupubs.onlinelibrary.wiley.com/doi/abs/10.1002/2014MS000416, 2015.

Landschützer, P., Gruber, N., Bakker, D. C. E., Schuster, U., Nakaoka, S., Payne, M. R., Sasse, T. P., and Zeng, J.: A neural network-based estimate of the seasonal to inter-annual variability of the Atlantic Ocean carbon sink, Biogeosciences, 10, 7793–7815, https://doi.org/10.5194/bg-10-7793-2013, 2013.

Landschützer, P., Gruber, N., Bakker, D. C. E., and Schuster, U.: Recent variability of the global ocean carbon sink, Global Biogeochem. Cycles, 28, 927–949, https://doi.org/10.1002/2014GB004853, 2014.

Landschützer, P., Gruber, N., and Bakker, D. C. E.: Decadal variations and trends of the global ocean carbon sink, Global Biogeochemical Cycles, 30, 1396–1417, https://doi.org/10.1002/2015GB005359, https://agupubs.onlinelibrary.wiley.com/doi/abs/10.1002/2015GB005359, 2016.

Landschützer, P., Gruber, N., and Bakker, D. C. E.: An updated observation-based global monthly gridded sea surface pCO2 and air-sea CO2 flux product from 1982 through 2015 and its monthly climatology (NCEI Accession 0160558). Version 2.2., 2017.

Landschützer, P., Gruber, N., Bakker, D. C. E., Stemmler, I., and Six, K. D.: Strengthening seasonal marine CO 2 variations due to increasing atmospheric CO 2, Nature Climate Change, 8, 146, https://doi.org/10.1038/s41558-017-0057-x, https://www.nature.com/articles/s41558-017-0057-x, 2018.

Landschützer, P., Ilyina, T., and Lovenduski, N. S.: Detecting Regional Modes of Variability in Observation-Based Surface Ocean pCO2, Geophysical Research Letters, 0, https://doi.org/10.1029/2018GL081756, https://agupubs.onlinelibrary.wiley.com/doi/abs/10.1029/2018GL081756, 2019.

Laruelle, G. G., Dürr, H. H., Slomp, C. P., and Borges, A. V.: Evaluation of sinks and sources of CO2 in the global coastal ocean using a spatially-explicit typology of estuaries and continental shelves, Geophysical Research Letters, 37, https://doi.org/10.1029/2010GL043691, https://agupubs.onlinelibrary.wiley.com/doi/abs/10.1029/2010GL043691, 2010.

Laruelle, G. G., Dürr, H. H., Lauerwald, R., Hartmann, J., Slomp, C. P., Goossens, N., and Regnier, P. a. G.: Global multi-scale segmentation of continental and coastal waters from the watersheds to the continental margins, Hydrology and Earth System Sciences, 17, 2029–2051, https://doi.org/https://doi.org/10.5194/hess-17-2029-2013, https://www.hydrol-earth-syst-sci.net/17/2029/2013/, 2013.

Laruelle, G. G., Landschützer, P., Gruber, N., Tison, J.-L., Delille, B., and Regnier, P.: Global high-resolution monthly pCO$_2$ climatology for the coastal ocean derived from neural network interpolation, Biogeosciences, 14, 4545–4561, https://doi.org/https://doi.org/10.5194/bg-14-4545-2017, https://www.biogeosciences.net/14/4545/2017/, 2017.

Laruelle, G. G., Cai, W.-J., Hu, X., Gruber, N., Mackenzie, F. T., and Regnier, P.: Continental shelves as a variable but increasing global sink for atmospheric carbon dioxide, Nature Communications, 9, 454, https://doi.org/10.1038/s41467-017-02738-z, https://www.nature.com/articles/s41467-017-02738-z, 2018.

Lauvset, S. K. and Gruber, N.: Long-term trends in surface ocean pH in the North Atlantic, Marine Chemistry, 162, 71–76, https://doi.org/10.1016/j.marchem.2014.03.009, https://www.sciencedirect.com/science/article/pii/S0304420314000607, 2014.

Lauvset, S. K., Gruber, N., Landschützer, P., Olsen, A., and Tjiputra, J.: Trends and drivers in global surface ocean pH over the past 3 decades, Biogeosciences, 12, 1285–1298, https://doi.org/https://doi.org/10.5194/bg-12-1285-2015, https://www.biogeosciences.net/12/1285/2015/, 2015.

Lima, F. P. and Wethey, D. S.: Three decades of high-resolution coastal sea surface temperatures reveal more than warming, Nat Commun, 3, 1–13, https://doi.org/10.1038/ncomms1713, https://www.nature.com/articles/ncomms1713, 2012.

Lind, S., Ingvaldsen, R. B., and Furevik, T.: Arctic warming hotspot in the northern Barents Sea linked to declining sea-ice import, Nature Clim Change, 8, 634–639, https://doi.org/10.1038/s41558-018-0205-y, https://www.nature.com/articles/s41558-018-0205-y, 2018.

Locarnini, R., Mishonov, A., Baranova, O., Boyer, T., Zweng, M., GarciA, H., Reagan, J., Seidov, D., Weathers, K., Paver, C., and Smoylar, I.: World Ocean Atlas 2018, Volume 1: Temperature, A. Mishonov Technical Ed., 2018.

Loose, B., McGillis, W. R., Schlosser, P., Perovich, D., and Takahashi, T.: Effects of freezing, growth, and ice cover on gas transport processes in laboratory seawater experiments, Geophysical Research Letters, 36, https://doi.org/10.1029/2008GL036318, https://agupubs.onlinelibrary.wiley.com/doi/abs/10.1029/2008GL036318, 2009.

Mehrbach, C., Culberson, C., Hawley, J., and Pytkowicz, R.: Measurement of the apparent dissociation constants of carbonic acid in seawater at atmospheric pressure, Limnol. Oceanogr., 18, 897–907, 1973.

Meyer, M., Pätsch, J., Geyer, B., and Thomas, H.: Revisiting the Estimate of the North Sea Air-Sea Flux of CO2 in 2001/2002: The Dominant Role of Different Wind Data Products, Journal of Geophysical Research: Biogeosciences, 123, 1511–1525, https://doi.org/10.1029/2017JG004281, https://agupubs.onlinelibrary.wiley.com/doi/abs/10.1029/2017JG004281, 2018.

Müller, J. D., Schneider, B., and Rehder, G.: Long-term alkalinity trends in the Baltic Sea and their implications for CO2-induced acidification, Limnology and Oceanography, 61, 1984–2002, https://doi.org/10.1002/lno.10349, https://aslopubs.onlinelibrary.wiley.com/doi/abs/10.1002/lno.10349, 2016.

Naegler, T.: Reconciliation of excess 14C-constrained global CO2 piston velocity estimates, Tellus B: Chemical and Physical Meteorology, 61, 372–384, https://doi.org/10.1111/j.1600-0889.2008.00408.x, https://doi.org/10.1111/j.1600-0889.2008.00408.x, 2009.

Nondal, G., Bellerby, R. G. J., Oldenc, A., Johannessena, T., and Olafssond, J.: Optimal evaluation of the surface ocean CO2 system in the northern North Atlantic using data from voluntary observing ships, Limnol. Oceanogr., 7, 109–118, 2009.

Omar, A. M., Thomas, H., Olsen, A., Becker, M., Skjelvan, I., and Reverdin, G.: Trend of ocean acidification and pCO2 in the northern North Sea, 2004-2015, Journal of Geophysical Research - Biogeosciences, 2019.

Oziel, L., Neukermans, G., Ardyna, M., Lancelot, C., Tison, J.-L., Wassmann, P., Sirven, J., Ruiz-Pino, D., and Gascard, J.-C.: Role for Atlantic inflows and sea ice loss on shifting phytoplankton blooms in the Barents Sea, Journal of Geophysical Research: Oceans, pp. 5121–5139, https://doi.org/10.1002/2016JC012582@10.1002/(ISSN)2169-9291.ARCTICJOINT, https://agupubs.onlinelibrary.wiley.com/doi/abs/10.1002/2016JC012582%4010.1002/%28ISSN%292169-9291.ARCTICJOINT, 2016.

5 Parard, G., Charantonis, A. A., and Rutgersson, A.: Using satellite data to estimate partial pressure of CO $_2$ in the Baltic Sea: PARTIAL PRESSURE OF CO $_2$ VARIABILITY, Journal of Geophysical Research: Biogeosciences, 121, 1002–1015, https://doi.org/10.1002/2015JG003064, http://doi.wiley.com/10.1002/2015JG003064, 2016.

Parard, G., Rutgersson, A., Raj Parampil, S., and Charantonis, A. A.: The potential of using remote sensing data to estimate air–sea CO₂ exchange in the Baltic Sea, Earth System Dynamics, 8, 1093–1106, 10 https://doi.org/10.5194/esd-8-1093-2017, https://www.earth-syst-dynam.net/8/1093/2017/, 2017.

Pierrot, D., Neill, C., Sullivan, K., Castle, R., Wanninkhof, R., Lüger, H., Johannessen, T., Olsen, A., Feely, R. A., and Cosca, C. E.: Recommendations for autonomous underway $p\mathrm{CO_2}$ measuring systems and data-reduction routines, Surface Ocean CO2 Variability and Vulnerabilities, 56, 512–522, https://doi.org/10.1016/j.dsr2.2008.12.005, 2009.

Rödenbeck, C., Keeling, R. F., Bakker, D. C. E., Metzl, N., Olsen, A., Sabine, C., and Heimann, M.: Global surface-ocean pCO2 and sea–air 15 CO2 flux variability from an observation-driven ocean mixed-layer scheme, Ocean Sci., 9, 193–216, https://doi.org/10.5194/os-9-193-2013, https://www.ocean-sci.net/9/193/2013/, 2013.

Rödenbeck, C., Bakker, D. C. E., Metzl, N., Olsen, A., Sabine, C., Cassar, N., Reum, F., Keeling, R. F., and Heimann, M.: Interannual sea–air CO$_2$ flux variability from an observation-driven ocean mixed-layer scheme, Biogeosciences, 11, 4599–4613, https://doi.org/https://doi.org/10.5194/bg-11-4599-2014, https://www.biogeosciences.net/11/4599/2014/bg-11-4599-2014.html, 2014.

20 Rödenbeck, C., Bakker, D. C. E., Gruber, N., Iida, Y., Jacobson, A. R., Jones, S., Landschützer, P., Metzl, N., Nakaoka, S., Olsen, A., Park, G.-H., Peylin, P., Rodgers, K. B., Sasse, T. P., Schuster, U., Shutler, J. D., Valsala, V., Wanninkhof, R., and Zeng, J.: Data-based estimates of the ocean carbon sink variability – first results of the Surface Ocean pCO$_2$ Mapping intercomparison (SOCOM), Biogeosciences, 12, 7251–7278, https://doi.org/https://doi.org/10.5194/bg-12-7251-2015, https://www.biogeosciences.net/12/7251/2015/, 2015.

Salt, L. A., Thomas, H., Prowe, A. E. F., Borges, A. V., Bozec, Y., and Baar, H. J. W. d.: Variability of North Sea pH 25 and CO2 in response to North Atlantic Oscillation forcing, Journal of Geophysical Research: Biogeosciences, 118, 1584–1592, https://doi.org/10.1002/2013JG002306, https://agupubs.onlinelibrary.wiley.com/doi/abs/10.1002/2013JG002306, 2013.

Schneider, B. and Müller, J. D.: Biogeochemical Transformations in the Baltic Sea: Observations Through Carbon Dioxide Glasses, Springer Oceanography, Springer International Publishing, https://www.springer.com/gp/book/9783319616988, 2018.

Sharples, J., Ross, O. N., Scott, B. E., Greenstreet, S. P. R., and Fraser, H.: Inter-annual variability in the timing of stratification and the 30 spring bloom in the North-western North Sea, Cont.Shelf Res., 26, 733–751, https://doi.org/10.1016/j.csr.2006.01.011, https://abdn.pure.elsevier.com/en/publications/inter-annual-variability-in-the-timing-of-stratification-and-the-, 2006.

Thomas, H., Bozec, Y., Elkalay, K., and Baar, H. J. W. d.: Enhanced Open Ocean Storage of CO2 from Shelf Sea Pumping, Science, 304, 1005–1008, https://doi.org/10.1126/science.1095491, https://science.sciencemag.org/content/304/5673/1005, 2004.

Thomas, H., Friederike Prowe, A. E., van Heuven, S., Bozec, Y., de Baar, H. J. W., Schiettecatte, L.-S., Suykens, K., Koné, M., Borges, 35 A. V., Lima, I. D., and Doney, S. C.: Rapid decline of the CO2 buffering capacity in the North Sea and implications for the North Atlantic Ocean, Global Biogeochemical Cycles, 21, https://doi.org/10.1029/2006GB002825, https://agupubs.onlinelibrary.wiley.com/doi/full/10.1029/2006GB002825, 2007.

van Heuven, S., Pierrot, D., Lewis, E., and Wallace, D.: {MATLAB} Program Developed for {CO}$_2$ System Calculations. {ORNL/CDIAC}-105b., 2009.

Wanninkhof, R.: Relationship between wind speed and gas exchange over the ocean revisited: Gas exchange and wind speed over the ocean, Limnology and Oceanography: Methods, 12, 351–362, https://doi.org/10.4319/lom.2014.12.351, http://doi.wiley.com/10.4319/lom.2014.12.351, 2014.

Weiss, R. F.: Carbon dioxide in water and seawater: The solubility of a non-ideal gas, Mar. Chem., 2, 203–215, 1974.

Wesslander, K., Omstedt, A., and Schneider, B.: Inter-annual and seasonal variations in the air–sea CO2 balance in the central Baltic Sea and the Kattegat, Continental Shelf Research, 30, 1511–1521, http://www.academia.edu/16389763/Inter-annual_and_seasonal_variations_in_the_air_sea_CO2_balance_in_the_central_Baltic_Sea_and_the_Kattegat, 2010.

Yasunaka, S., Siswanto, E., Olsen, A., Hoppema, M., Watanabe, E., Fransson, A., Chierici, M., Murata, A., Lauvset, S. K., Wanninkhof, R., Takahashi, T., Kosugi, N., Omar, A. M., Heuven, S. v., and Mathis, J. T.: Arctic Ocean CO$_2$ uptake: an improved multiyear estimate of the air–sea CO$_2$ flux incorporating chlorophyll *a* concentrations, Biogeosciences, 15, 1643–1661, https://doi.org/https://doi.org/10.5194/bg-15-1643-2018, https://www.biogeosciences.net/15/1643/2018/, 2018.